JVST B
Journal of Vacuum Science & Technology B

Detection of some amino acids with modulation-doped and surface-nanoengineered GaAs Schottky P-I-N diodes

Cite as: J. Vac. Sci. Technol. B **38**, 054002 (2020); https://doi.org/10.1116/6.0000186
Submitted: 12 March 2020 . Accepted: 14 July 2020 . Published Online: 17 August 2020

Tamador Alkhidir, Maguy Abi Jaoude, Deborah L. Gater, Christopher Alpha, and A. F. Isakovic

JVST B
Journal of Vacuum Science & Technology B

ARTICLE

avs.scitation.org/journal/jvb

Detection of some amino acids with modulation-doped and surface-nanoengineered GaAs Schottky P-I-N diodes

Cite as: J. Vac. Sci. Technol. B 38, 054002 (2020); doi: 10.1116/6.0000186
Submitted: 12 March 2020 · Accepted: 14 July 2020 ·
Published Online: 17 August 2020

Tamador Alkhidir,[1] Maguy Abi Jaoude,[1] Deborah L. Gater,[2] Christopher Alpha,[3] and A. F. Isakovic[1,4,a)]

AFFILIATIONS

[1]ECE Dept., Chemistry Dept., Khalifa University of Science and Technology, Abu Dhabi 127788, United Arab Emirates
[2]Institute of Education, University College London, London WC1E 6BT, United Kingdom
[3]CNF, Cornell University, Ithaca, New York 14850
[4]Dept. of Physics and Astronomy, Colgate University, Hamilton, New York 13346

Note: This paper is part of the Special Topic Collection from the 47th Conference on the Physics and Chemistry of Surfaces and Interfaces (PCSI-47) 2020 meeting.

[a)]**Author to whom correspondence should be addressed:** aisakovic@colgate.edu and iregx137@gmail.com

ABSTRACT

Most current techniques for analyzing amino acids require substantial instrumentation and significant sample preprocessing. In this study, we designed, fabricated, and tested a scalable diode-based microdevice that allows for direct sensing of amino acids. The device is based on modulation-doped GaAs heterostructure with a Schottky contact on one side. The relatively high mobility and relatively small dielectric constant of GaAs are naturally helpful in this problem. We also paid attention to a proper etching procedure allowing for substantial modification of the surface properties, thereby further boosting the sensing performance. Transport data (I-V, differential conductance) are presented for three qualitatively different classes of amino acids (i.e., nonpolar with aliphatic R-group, polar uncharged R-group, and charged R-group) with glycine, cysteine, and histidine as specific examples, respectively. The conductance for the GaAs-amino acid interface measured using a scanning tunneling microscope (STM) was previously reported to have distinct spectral features. In this paper, we show that measuring the differential conductance of a GaAs diode, whose surface is in direct contact with an aqueous solution of amino acid, is a simple methodology to access useful information, previously available only through sophisticated and equipment-demanding STM and molecular electronics approaches. Density functional theory calculations were used to examine which adsorption processes were likely responsible for the observed surface conductance modification. Last, in future and ongoing work, we illustrate how it might be possible to employ standard multivariate data analysis techniques to reliably identify distinct (95%) single amino acid specific features in near-ambient differential conductance data.

I. INTRODUCTION

The rapid and accurate detection of small biomolecules such as short peptides and single amino acids is required in various contexts.[1–4] The variation in semiconductor surface properties, often in the form of modification of the density of states, due to amino acid chemisorption, is significant and promotes the development of sensitive selective biosensors.[5] Therefore, some current research initiatives in biosensing focus on utilizing semiconductor devices for their easy deployment, simplicity, portability, and scalability down to submicrometer and, where feasible, nanoscale dimensions. The current detection methods for biosubstances using semiconductors or metallic materials can be classified as classical and quantum-based.[6,7]

In the quantum detection approach, the conductance measured from molecules sandwiched between two metallic electrodes exhibits statistical variations specific to each molecule being tested. The vibrational modes of the tested molecules introduce additional discrete energy levels affecting the electron transport. Understanding

the electronic quantum transport through organic materials is not straightforward. However, with the advent of machine learning and multivariate analysis techniques, vital information regarding the molecular conformation can be extracted from the stochastic peaks in the measured conductance,[8] where the deduced information is similar to that reported by optical spectroscopy techniques such as Fourier transform infrared (FTIR) and Raman. Although the quantum approach gives a thorough understanding of the molecular conformation and displays very high accuracy in recognizing different molecules, it requires complex setup, low temperature, and high vacuum in most cases, which makes it not practical for quick diagnosis and integration into handheld or small table-top devices.

In the classical approach, the semiconductor devices and/or samples tested are functionalized with receptor/binder materials (e.g., enzymes)[9] to enable the sensing via the measurement of current-,[2] capacitance-,[10] or resistance-change,[6] which are then directly correlated to the concentration of the species of interest. One faces here two contrasting tendencies. On one hand, the electrical characteristics of semiconductor devices are highly sensitive to variations in sample volume and require sensitive, selective materials that are highly prone to biofouling.[6,11] On the other hand, the appealing benefit in using semiconductor devices is the user-friendly setup and configuration, where relatively minor nanofabrication efforts are needed (etched microdevice, patterned electrodes, and a simple readout circuitry). To this end, we combined the ideas of both classical and quantum approaches, to balance scientific reliability, efficiency, and practicality.

Research questions we address here are: (1) is it possible to distinguish between different amino acids in contact with the same GaAs interface, based on I-V curves?; (2) how are partial charges specific to individual amino acids?; (3) what are the likely binding mechanisms (individual amino acid to GaAs)?; and (4) to what extent one can use differential conductance data? We show how it is possible to distinguish between separate aqueous solutions of the amino acids in interface contact with the GaAs Schottky PIN diode through I-V and differential conductance measurements. As examples, we used glycine, *L*-cysteine, and *L*-histidine, which each fall into a different amino acid category. Glycine is nonpolar, *L*-cysteine is polar and contains a side chain thiol group, and *L*-histidine contains a side chain base group. Transport data analysis has led to the study of mutual dependencies between several variables (*p*H factor, partial charge, conductivity). Beyond I-V transport data, we have used density functional theory (DFT) simulations to elucidate most likely binding mechanism for each amino acid (in this context, modification of surface density of states). Last, we propose and show initial results of the application of multivariate data analysis (MVA) to distinguish between the different amino acids solutions, presented in Sec. IV.

II. METHODOLOGY AND EXPERIMENT

A. Sensor structure

The array of microsensor diodes we developed here is based on a P-I-N trilayer of GaAs, combined with Schottky diode. Specifically, a metallic (Ti-Au bilayer) was deposited on top of the (100) oriented AlGaAs (n+)/GaAs (I)/AlGaAs (p++) structure (Fig. 1). The layers of AlGaAs/GaAs were doped to create a [n-i-p]

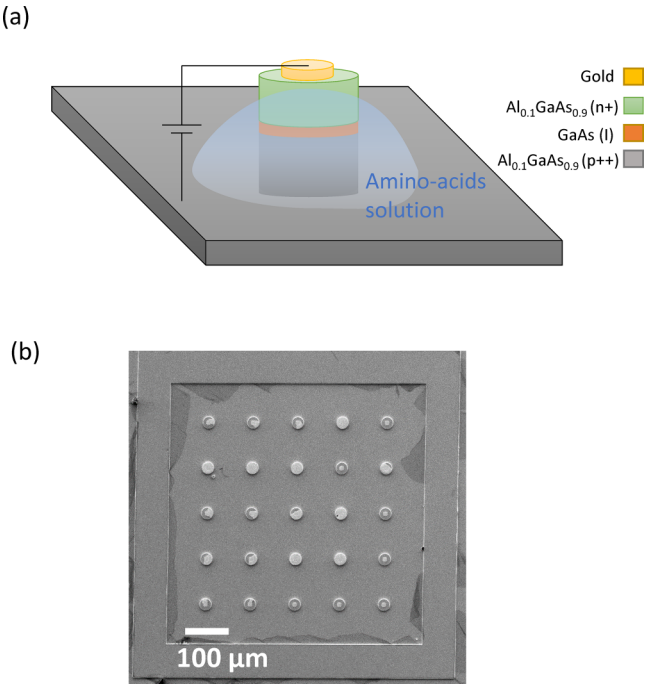

FIG. 1. (a) GaAs Schottky diode schematic and (b) scanning electron micrograph of the GaAs pillars. The structure consists of gold electrodes grown on top of an n-doped $Al_{0.1}Ga_{0.9}As$ layer, followed by a 10 nm quantum well of i-GaAs, and then a p-doped $Al_{0.1}Ga_{0.9}As$. Last, the substrate is a highly doped $Al_{0.1}Ga_{0.9}As$ substrate to facilitate ohmic connection. Through conventional photolithography steps and dry reactive ion etching, the AlGaAs/GaAs/AlGaAs stack was patterned into a pillar format. The structure consists of 25 GaAs pillars with 15 μm radius and 4 μm height with 100 μm separation between each pillar.

structure ($N_D = 7 \times 10^{16}$ cm^{-3}, $N_A = 2 \times 10^{18}$ cm^{-3}). The substrate is also p++ doped, so it creates a near ohmic contact.

The "nanoengineering of surface" we refer to in the title was achieved by a specific plasma etching process, programmed to have alternating short periods of over- and underetch (the process known as "cyclc etch"), thus controllably creating the surface that allows a good, uniform adsorption of the solution on the microscale. It is well known[12–14] that GaAs and related surfaces are prone to oxidation in water solutions. To prevent accumulation of oxide, the surface of devices (Fig. 1) is cleaned with an HCl based solution and blow dried after each measurement. While there is no doubt that some oxidation occurs, we emphasize that transport data presented here are repeatable, obtained under same condition for all measurements, and easily distinguishable between different amino acids.

B. Solutions preparation

A phosphate buffer saline (PBS) solution (Sigma-Aldrich, St. Louis, MO, USA) was used to prepare 0.1M solutions of *l*-histidine (Sigma-Aldrich, St. Louis, MO, USA), *l*-cystine (Sigma-Aldrich, St. Louis, MO, USA) and glycine (Sigma-Aldrich,

St. Louis, MO, USA). The PBS buffer solution was prepared in de-ionized water yielding 0.01M phosphate buffer and 0.0027M potassium chloride and 0.137M sodium chloride at room temperature. The *p*H of amino acid solutions was adjusted to the desired level within the range 4.0–9.0 using small quantities of concentrated NaOH and HCl. During transport measurements, the amino acid solution is in contact with N-I-P structure.

C. IV measurement

The current-voltage (IV) curves for the GaAs Schottky diode in contact with different amino acid solutions (*L*-histidine, *L*-cysteine, glycine) were measured at room temperature, using a Keithley characterization tool (4200-SCS), with one probe attached to the metallic layer atop of the GaAs Schottky pillar, and the other was in contact with the substrate layer. The measurements were conducted by adding small droplets of the analyte solution into the walled well surrounding the device pillars, allowing the pillar to become immersed in the solution, while avoiding wetting the upper surface of the device or the metallic electrode. The measurement was repeated eight times with dual sweep, resulting in 48 IV curves for each amino acid at each specific *p*H value.

D. Transport data processing

The data for the IV measurement was averaged and smoothened using the MATLAB function ("smooth" with the "rlowess" method) as shown in Figs. 2(a)–2(c). The conductance (dI/dV) and differential conductance (d^2I/dV^2) were found using standard AC modulated methods. The differential conductance d^2I/dV^2 was normalized to allow easier comparison between the different amino acid solutions.

E. Quantum transport simulation

Quantum transport models were previously used to understand the chemisorption related processes and the electron transport in complex systems similar to ours.[15] Depending on the assumptions made during the modeling of the system, one-dimensional (or a near 1D) approach based on the Landauer–Büttiker formalism might be useful. We find it as a good initial approach as the disproportionately high conduction relevant to the sensing of molecules external to GaAs comes from the approximately 1D layer interfacing GaAs and adsorbed amino acid. Landauer–Büttiker formalism is given by Eq. (1),

$$I(V) = \int_{-\infty}^{\infty} T(E)[f_L(E) - f_R(E)]dE,$$
$$f_{L(R)} = [\exp\left[\frac{(E-\mu_{L(R)})}{k_BT}\right] + 1]^{-1}, \quad (1)$$

where $\mu_{L(R)}$ are the electrochemical potentials of the left and right electrodes, respectively. $f_{L(R)}$ is the Fermi–Dirac distribution at the left and right electrodes, and $T(E)$ is the transmittance factor,[16]

$$T(E) = Tr(\Gamma_L G_L^r \Gamma_R G_c^a). \quad (2)$$

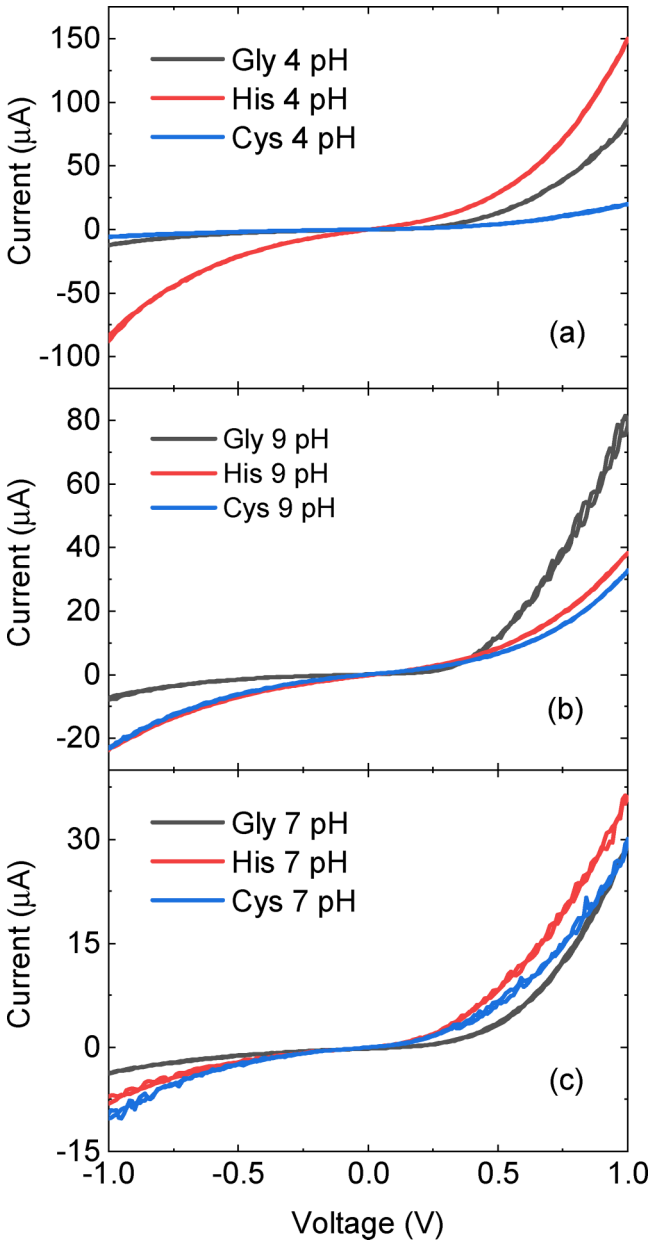

FIG. 2. GaAs Schottky diode current for Gly, His, and Cys amino acids at different *p*Hs: 4, 7, and 9.

$\Gamma_{L,R}$ is the coupling matrix that described the right and the left electrodes, and G is the Green function associated with the conductor. A slab from the 76 atoms of GaAs was constructed in a "lead-conductor-lead" geometry format, where the middle part of the slab is modeled as a nondispersive conductor sandwiched between two symmetrical leads. Electrons hop from the lead to the empty energy bands in the conductor with a transmission

probability called quantum conductance. The quantum conductance was found through using the following approach.

First, a universal force field simulation in Avogadro software was used to find the relative location between the molecules and the surface of GaAs that minimizes the energy of the system. This optimized geometry was passed to QUANTUM ESPRESSO (Refs. 17 and 18) by setting 80 Ry cut off energy for the plane wave basis and Gaussian smearing. The QUANTUM ESPRESSO code was used to find the energy bands for electrons using DFT by solving the Kohn–Sham equations. Wannier90 package[19] was used to convert the Bloch plane states found using QUANTUM ESPRESSO to MLWF (maximally localized Wannier functions) bases. The Hamiltonian in MLWF describing the quantum conductance is then solved by constructing the left and the right leads. The method details mirror the efforts in Ref. 20 and related references.[21–24] We caution that we are using a simplified model system in the form of bias lead–GaAs–bias lead and a single amino acid molecule, instead of a more realistic AlGaAs–GaAs–AlGaAs N-I-P system with a larger number of atoms and with a water solution of amino acid. This simplification is justified as long as one is primarily low bias device functioning.[25]

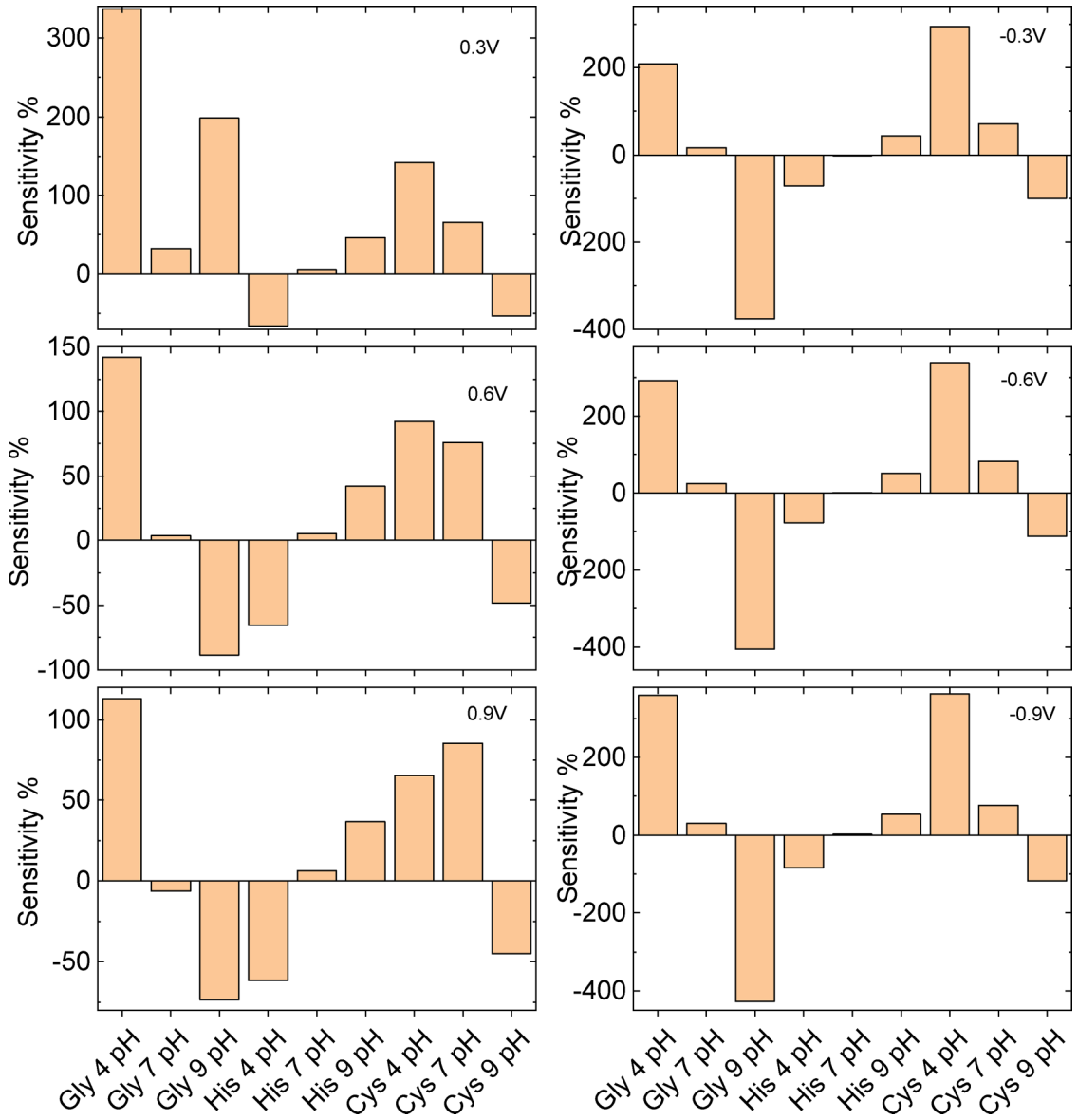

FIG. 3. Sensitivity calculation $S = (I_{amino} - I_{GaAs})/I_{GaAs}$ at different bias conditions and different *p*Hs.

III. RESULTS AND DISCUSSION

A. Conductivity and partial charge versus *p*H factor

Figure 2 shows raw data current-voltage curves for the GaAs diode with different amino acids at different *p*H levels (4, 7, and 9). Additional data are available for more amino acids and for additional values of *p*H factor, but do not substantively change the discussion here. The bonding between GaAs surface and protons (or functional groups from amino acid) introduces variation in the surface charge density.[5] Variations in the surface charge density modify the electronic distribution (N_e) and ultimately the measured conductance ($\sigma \sim N_e\mu_e$, μ_e is the mobility). The partial charges for each amino acid functional group x, at any given *p*H is

$$p_x = \frac{n}{1 + 10^{n(\mathrm{pH} - pk_x)}}, \tag{3}$$

where n is the sign describing the polarity of the functional group at the different *p*H. Therefore, the total charge is the combination of partial charge for the carboxyl group, amino group and the side group ($P_T = \sum p_x$) [Fig. 4(a)]. The partial charge equation is found by rearranging the Henderson–Hasselbalch equation.[26]

We note the asymmetry of I-V curves upon bias voltage inversion offers useful information, similar to studies reported in Refs. 27 and 24. Essentially, analysis of either I-V curves or differential conductance (here, both), points toward energy levels where main conduction channels occur. Naturally, varied bias voltage and polarity changes put emphasis on various species whose adsorbance to the surface modifies conductivity, thereby altering the I-V curve and leading to the relevant signal in a diode-based sensor. Following I-V curves raw data, we calculated relative sensitivity (change in current with an amino acid present relative to GaAs only curve at a fixed voltage) for a number of voltage values. The sensitivity values are shown in Fig. 3 for selected voltages where one might choose to calibrate the device for different amino acids. Additional analysis is provided later in the text.

Using Poisson's equation solver for semiconductor devices (Medici, Synopsys Inc., USA), the surface charge induced by the functional group of the amino acids was simulated. Figure 4(b) shows the conductance (dI/dV) plotted against the partial charge in reference to bare GaAs Schottky diode for both the experiment (full symbols) and the simulation (open symbols). The partial charge and the computed charge density were mapped as following:

$$Q_s \sim P_T N_A M_x, \tag{4}$$

where N_A is the Avogadro number and M_x is the solution concentration per volume (cm^{-3}). It is clear from Fig. 3(b) that there are deviations between the simulation and the experiment. This demonstrates that the interaction between the amino acids and the GaAs surface cannot be solely explained by the change in the charge distribution. Some amino acids bind via head-tail monolayer configuration [via carboxyl groups at the surface of GaAs (Ref. 1)], while for others, the binding to GaAs surface may occur through other functional groups. For example, *L*-cysteine adsorption to the GaAs surface occurs primarily through the thiol group

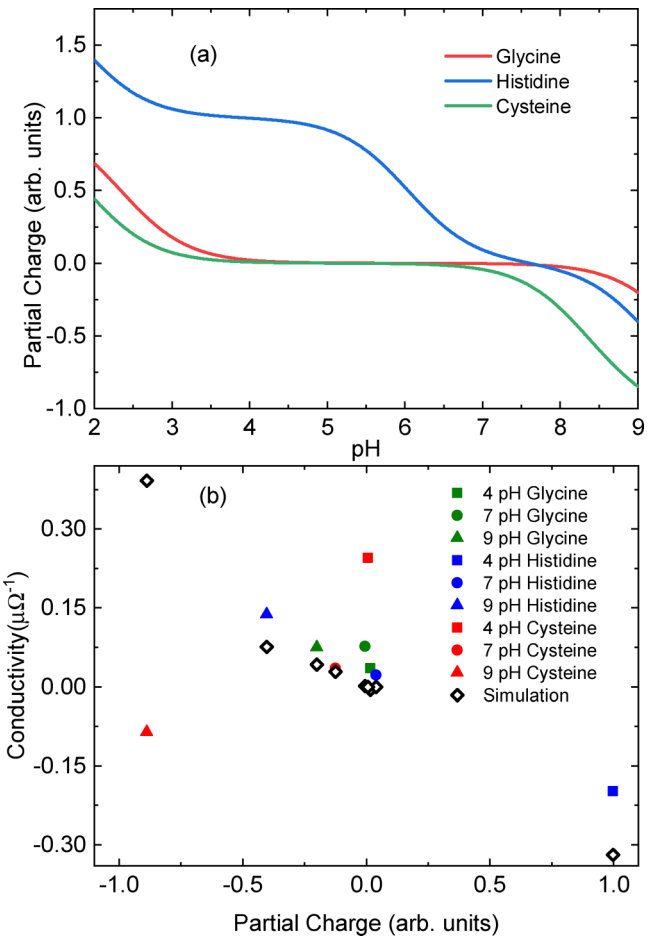

FIG. 4. (a) Partial charge values for the different amino acids at different *p*Hs. (b) Conductivity as a function of partial charge; the highest deviation between experiment and simulation is seen by *L*-cysteine. This behavior is likely caused by the As–S bond.

(As–S bond).[28] Appearance of broken Al, Ga, and As bonds on the surface of the device likely contributes to preferential bonding along p++, n+, or undoped portions of the heterostructure. It remains to be seen how does performance of modulation-doped III–V heterostructures compare with the use of graphene and its derivatives, such as graphene oxide in detection of amino acids, as one can foresee greater flexibility of graphene derivatives from the materials stand point, and easier microdevice realization from the standpoint of III–V heterostructures. Regardless of the details of mechanism, the conformation of the amino acids at the GaAs surface affects the electron transport. The differences in adsorption to p-doped and n-doped section may be partially responsible for observed variations between amino acids related surface charge variations. This is, in part, intuitively clear from the changes in the sign of deviation, perhaps most obviously for cysteine in Fig. 4(b).

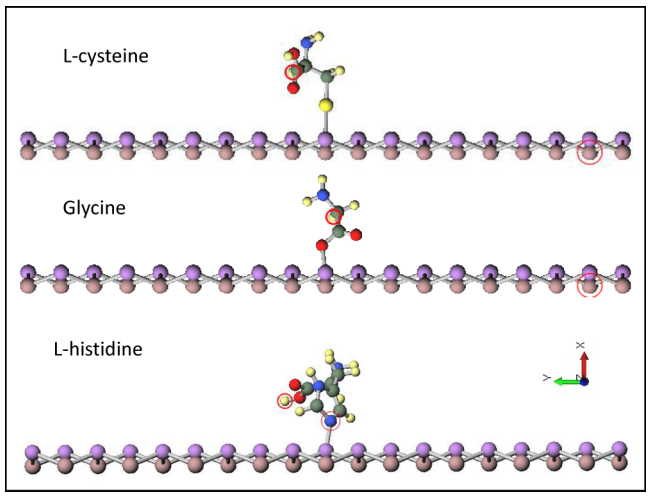

FIG. 5. Molecular configuration of *L*-cysteine, *L*-histidine, and glycine on top of GaAs 2D slab. *L*-cysteine is bonded to GaAs through sulfur atom, *L*-histidine is bonded to GaAs through nitrogen of the imide group, and glycine is bonded to GaAs through carboxyl group.

B. Adsorbance of functional groups onto GaAs

In order to quantify the origin of the peaks in the differential conductance, we have used DFT to model the effect of amino acid adsorption at GaAs on electron transport. We used the Projected Augmented Wave (PAW) pseudopotential with the Perdew-Burke-Ernzerhof (PBE) functional. The convergence threshold was set at 1e−6 Ry, and we used unit cell $46 \times 21.5 \times 10.9$ A^3. To understand the reaction of the amino acids with GaAs, a conformation analogous to Ardalan *etal*.. for silicon[29] is used, except that we account for the two different bonding locations, arsenic and gallium. Figure 5 shows a sample of the molecular adsorption study of amino acids on the GaAs surface. To study the preferable location, the binding energy for GaAs, with the different amino acids, was found by calculating the difference between the combined structure and the isolated case; energy was calculated using self-consistent field calculation in QUANTUM ESPRESSO,

$$E_{\text{binding}} = E_{\text{GaAs+Amino}} - E_{\text{GaAs}} - E_{\text{Amino}}. \quad (5)$$

TABLE I. Binding energy and bond length for amino acids adsorbed at GaAs.

Configuration	Binding energy (eV)	Bond length (Å)
His-GaAs(As)	−0.3987	1.896
Cys-GaAs(As)	−0.9621	2.254
Gly-GaAs(As)	−0.8133	1.808
His-GaAs(Ga)	−0.3337	1.900
Cys-GaAs(Ga)	15.84	2.250
Gly-GaAs(Ga)	12.69	1.821

Table I shows the binding energy for the different amino acids bonded through gallium and arsenic. The positive binding energy indicates unstable confirmation. Therefore, the results in Table I generally suggest that arsenide atom is a more preferred location for amino acids bonding. The latter remark coincides well with the results reported in Ref. 30 that indicates adsorption location for hydrogen and sulfur is through arsenide atom. Our work points toward the glycine bonding through As-H, and *L*-histidine bonding through As–N bond (N from the imide group), and *L*-cysteine bonding with GaAs surface through As–S bond. For clarity, the optimized binding energies and bond lengths between GaAs slab and amino acids are shown in Table I.

C. Transport simulation results

Figure 6 shows the calculated density of states for GaAs slab with assignment of individual As and Ga bonds (s orbital energy for cation ε_s^{Ga}, s orbital energy for anion ε_s^{Aa} and p orbital energy for anion ε_p^{As}) and individual antibonding and bonding energy for GaAs bonds (σ bond hopping integrals ssσ and psσ).[31] The 2D slab was constructed to understand the effect of adsorbing amino acids at the GaAs surface. The density of states has some broad similarities to bulk GaAs,[32,33] but is clearly specific to dimensionally constrained cases. In low energy device design, the shaded area in Fig. 5 is of particular interest, so we calculated the conductance in that energy range (and shifted the zero energy level to the valence band). Differences and similarities in conductance between the three adsorbed amino acids are illustrated in Fig. 7. Chemical

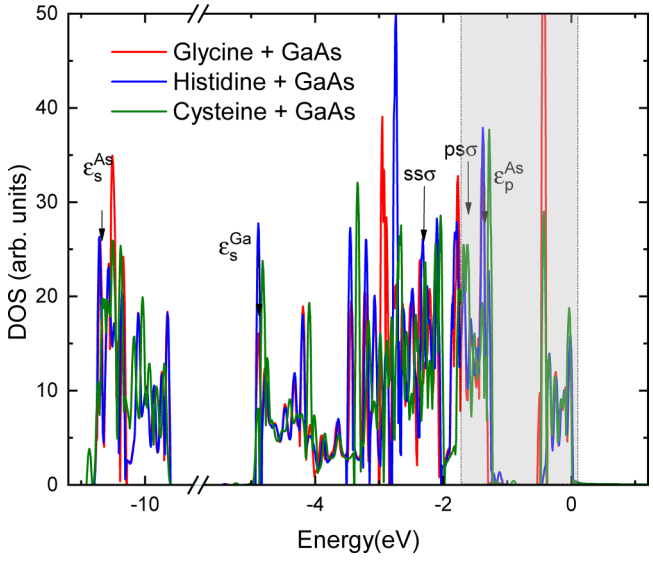

FIG. 6. Density of states for GaAs 2D slab, without and with *L*-histidine, *L*-cysteine, and glycine, with the assignment of individual As and Ga bonds (s orbital energy for cation ε_s^{Ga}, s orbital energy for anion ε_s^{As}, and p orbital energy for anion ε_p^{As}) and individual antibonding and bonding energy for GaAs bond (σ bond hopping integral ssσ and psσ). The shaded area is associated with the range of interest for conductance transmission simulation.

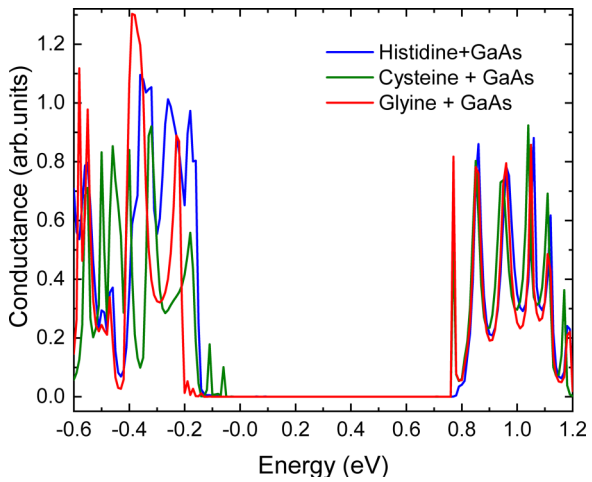

FIG. 7. Transmission coefficient (quantum conductance) for GaAs 2D slab with *L*-histidine, *L*-cysteine, and glycine. The quantum conductance for all the analysis was plotted to have the valence energy to be at zero energy level.

adsorption affects electron transport in the present consideration, and one can expect additional quantitative modifications after improving the method of how to account for inelastic effects, something that current literature does on case-by-case basis.

IV. ONGOING AND FUTURE WORK

Figure 8 shows the peaks in the differential conductance of IV curves for multiple measurements. The unique peaks in the amino acids differential conductance were previously reported to be measured using scanning tunneling microscope (STM) or nanogap configuration.[34] Those peaks are associated with the different vibrational modes of adsorbed molecules. By locating those peaks, the configuration and the structure of the hybrid [amino acid + surface GaAs layer(s)] at the interface could be understood. Unlike STM measurements, our proposed semiconductor device provides easy setup configuration without the need for additional components that are required in STM, such as a vacuum chamber, a low temperature, and a nanoscale tip. At the same time, one needs to be aware of alternative sources to the peaks in the differential conductance, which are attributed to noise originating in (a) electron

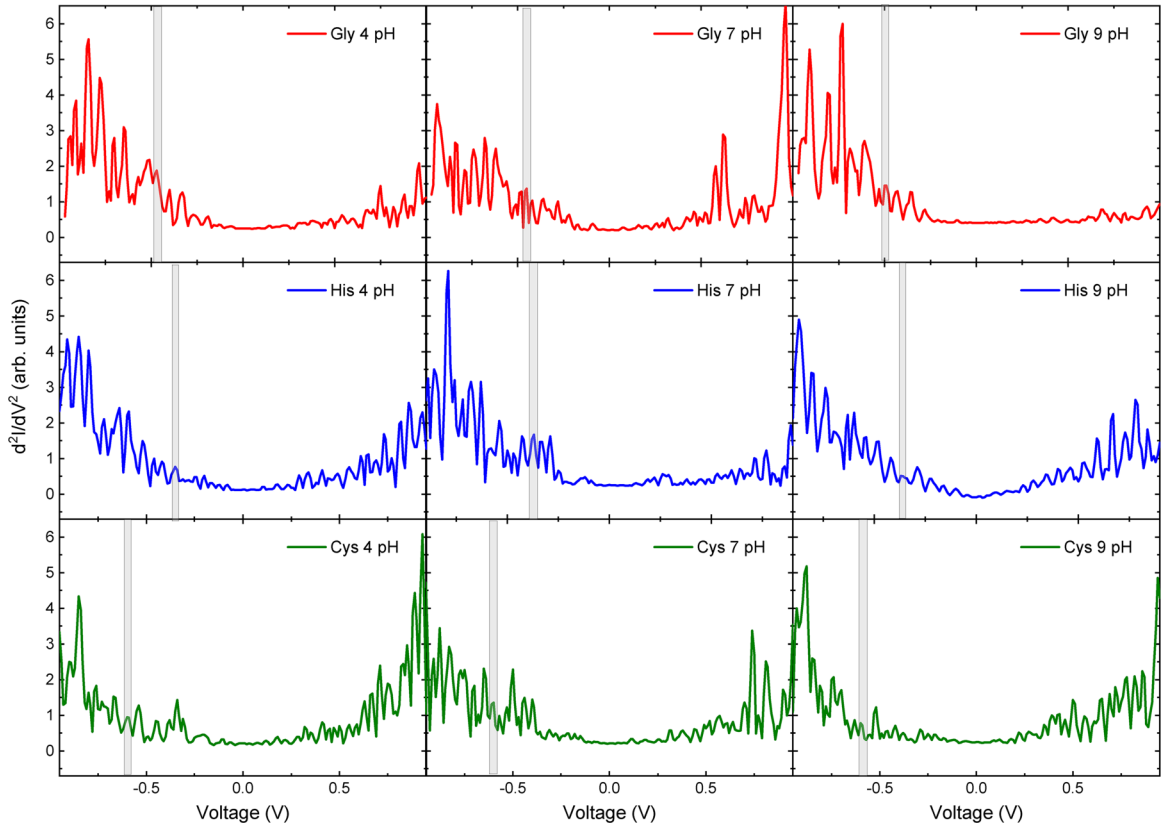

FIG. 8. Differential conductance d^2I/dV^2 for glycine, *L*-histidine, and *L*-cysteine solution. A number of unique features from each panel of this plot was extracted and fed to the MVA model to classify the amino acids.

trapping and detrapping at the surface of GaAs, (b) tunneling, and (c) thermal activation and random walks of electrons. Some of these peaks need to be understood in the context that, in the first approximation, electronic noise is inversely proportional to energy barrier height, which is affected by the different discrete energy levels associated (ϕ_B) with the vibrational modes for the tested molecules $S_n \propto \sum \frac{1}{\phi_B - V}$.[35] So, while "ease of testing" motivates the approach we took here, such an approach is not without weaknesses, in part because the peaks in the differential conductance are a combination of quantum transport behavior and noise related to electron transport.[35]

Here, we elaborate on the details of the procedure. The Hilbert transform was used to isolate the envelop governing the peaks of d^2I/dV^2. Then, the peaks were detected above certain threshold defined by twice the standard deviation of the current measurement (result is not significantly affected by choosing somewhat different thresholds). These latter steps are common in analysis of similar curves obtained by STM, so we felt they are applicable here, for the sake of future comparisons. For classifying the differential conductance data, Fischer discriminant analysis (FDA) was found using "fitcdiscr" function with discriminant type "pseudoQuadratic," while principal component analysis (PCA) was implemented using "pca" function in MATLAB. Figure 9 illustrates the block diagram of the MVA-based approach used to classify the amino acids tested here. It is known that GaAs surface chemisorption is sensitive to variation in the vibrational modes due to the adsorption of molecular species. For example, x-ray photoelectron spectroscopy data for GaAs with water reveals shift in the As 2p due to the formation of As–H.[36] In a separate study, the FTIR peak assigned to the amino group is found shifted due to its adsorption at the GaAs surface.[37] Therefore, cross correlation between the differential conduction of the bare Schottky GaAs and those of the diode in contact with the amino acids can quantify the modification to the GaAs chemisorption. Cross correlation returns the similarity between a vector and shifted copies from another vector as a function of the shift. This technique isolates similar features in the conductance measurement even if they are shifted in respect to bare GaAs conductance measurement. Since we hypothesize that the conformation of amino acids at GaAs surface induces additional peaks in the differential conductance, the voltages at which peaks occur were regarded as another main feature for classifying amino acids. Then, the smoothed data for the differential conductance and cross correlations were fed to PCA to reduce the dimensionality of the data and to extract the strongest relevant features. Our analysis indicates that first seven principle components need to be counted as most significant ones from the differential conductance and the cross correlation. Those principle components and the voltages where the peaks occur were passed to the FDA classification module. The analysis of the 144 IV curves for the different amino acids at the different pH was randomized before feeding to the FDA model, in order not to bias the model. The model yields 95% accuracy in tenfold cross validation.

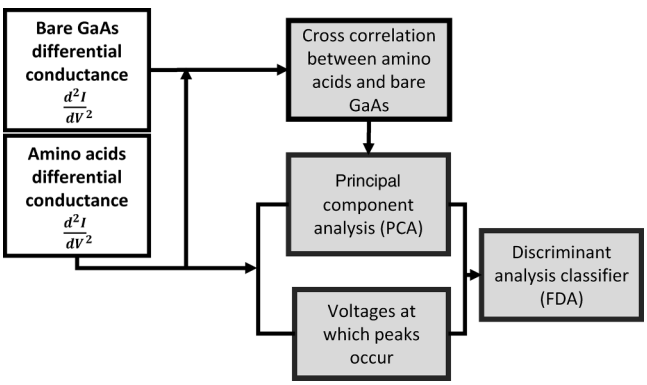

FIG. 9. Systematic diagram for the MVA-based approach for classifying the amino acids features in the differential conductance. Cross correlation, PCA, and FDA were used to classify the amino acids from the differential conductance.

When looking at Fig. 7, it is important to emphasize that it is not always the voltage values where the highest values in differential conductance peaks occur that are most statistically significant voltage values relevant to identification of an individual amino acid. This is pointed in Fig. 7 by using a narrow gray rectangle at some voltage values where differential conductance has moderate values.

V. CONCLUSION

Our answers to the research questions from Sec. I are the following: (1) It is indeed possible to distinguish individual amino acids in contact with GaAs surface via I-V measurements. (2) Partial charges in the range $[-1, +1.5]$ can be identified while varying pH factor of amino acid solutions in the range [4, 9]. (3) The most likely bonding sites are (a) L-cysteine bonds to GaAs surface via a sulfur atom, L-histidine via nitrogen of the imide group, and glycine bonds via the carboxyl group. (4) Differential conductance data are useful in identifying specific voltage values at which characteristic peaks for each amino acid characteristic occur. The pairs (voltage, diff. conductance peak) could be identified for each amino acid with a very good reliability, and further device and analysis improvements will likely increase it.

The next steps will involve: (a) fine tuning the device design (doping profile, thicknesses of layers, etc.) and (b) improving the MVA approach. The ultimate goal is the identification of individual amino acids in mixed solutions and quantification of their relative concentrations. In addition, future handheld devices require integration with microfluidics for fine pico-volume control. (c) Additional research is needed to ascertain precise and specific mechanisms of amino acids interacting with the AlGaAs/GaAs surface, and spectroscopic techniques, such as high resolution x-ray absorption and IR/Raman, will be used.

ACKNOWLEDGMENTS

This work was supported in part by the ADEC-AARE 2015 Grant and the Mubadala-SRC MEES I-/II Programs. This work was performed in part at the Cornell NanoScale Science and Technology Facility (CNF), a member of the National Nanotechnology Coordinated Infrastructure, which is supported by the National Science Foundation (NSF) (Grant No. NNCI-1542081). T.A. acknowledges initial support from the Biotechnology Centre at Khalifa University, Abu Dhabi, UAE.

REFERENCES

[1]S. R. Whaley, D. English, E. L. Hu, P. F. Barbara, and A. M. Belcher, Nature **405**, 665 (2000).
[2]G. L. Luque, N. F. Ferreyra, and G. A. Rivas, Talanta **71**, 1282 (2007).
[3]E. Estephan, C. Larroque, N. Bec, P. Martineau, F. J. Cuisinier, T. Cloitre, and C. Gergely, Biotechnol. Bioeng. **104**, 1121 (2009).
[4]U. O. S. Seker and H. V. Demir, Molecules **16**, 1426 (2011).
[5]M. Matmor and N. Ashkenasy, J. Am. Chem. Soc. **134**, 20403 (2012).
[6]D. Bavli, M. Tkachev, H. Piwonski, E. Capua, I. D. Albuquerque, D. Bensimon, G. Haran, and R. Naaman, Langmuir **28**, 1020 (2012).
[7]W.-Q. Li, B. Huang, M.-L. Huang, L.-L. Peng, Z.-W. Hong, J.-F. Zheng, W.-B. Chen, J.-F. Li, and X.-S. Zhou, Sensors **17**, 811 (2017).
[8]T. Albrecht, G. Slabaugh, E. Alonso, and S. M. R. Al-Arif, Nanotechnology **28**, 423001 (2017).
[9]M. S. Alaejos and F. J. Garcia Montelongo, Chem. Rev. **104**, 3239 (2004).
[10]V. Ijeri, F. Vocanson, C. Martelet, and N. Jaffrezic-Renault, Electroanalysis **19**, 510 (2007).
[11]Q. Zhang, D. Zhang, Y. Lu, G. Xu, Y. Yao, S. Li, and Q. Liu, Biosens. Bioelectron. **77**, 963 (2016).
[12]C. L. McGuiness, *et al.*, ACS Nano **4**, 3447 (2010).
[13]C. L. McGuiness, A. Shaporenko, M. Zharnikov, A. V. Walker, and D. L. Allara, J. Phys. Chem. C **111**, 4226 (2007).
[14]C. L. McGuiness, D. Blasini, J. P. Masejewski, S. Uppili, O. M. Cabarcos, D. Smilgies, and D. L. Allara, ACS. Nano. **1**, 30 (2007).
[15]R. Zhiani, Appl. Surf. Sci. **409**, 35 (2017).
[16]R. G. Sarmento, N. F. Frazao, and A. Macedo-Filho, Phys. Lett. A **381**, 276 (2017).
[17]P. Giannozzi *et al.*, J. Phys. Condens. Matter **21**, 395502 (2009).
[18]P. Giannozzi *et al.*, J. Phys. Condens. Matter **29**, 465901 (2017).
[19]A. A. Mostofi, J. R. Yates, G. Pizzi, Y.-S. Lee, I. Souza, D. Vanderbilt, and N. Marzari, Comput. Phys. Commun. **185**, 2309 (2014).
[20]M. Shelley, N. Poilvert, A. A. Mostofi, and N. Marzari, Comput. Phys. Commun. **182**, 2174 (2011).
[21]P. Singla, M. Riyaz, S. Singhal, and N. Goel, Phys. Chem. Chem. Phys. **18**, 5597 (2016).
[22]P. Zhang, Z. Wang, L. Liu, L. H. Klausen, Y. Wang, J. Mi, and M. Dong, Appl. Mater. Today **14**, 151 (2019).
[23]S. J. Rodríguez, L. Makinistian, and E. A. Albanesi, Appl. Surf. Sci. **419**, 540 (2017).
[24]S. J. Rodríguez and E. A. Albanesi, Phys. Chem. Chem. Phys. **21**, 597 (2019).
[25]D. Vasileska, S. M. Goodnick, and G. Klimeck, *Computational Electronics: Semiclassical and Quantum Device Modeling and Simulation* (CRC, Boca Raton, 2017).
[26]J. C. Cameselle, J. M. Ribeiro, and A. Sillero, Biochem. Educ. **14**, 131 (1986).
[27]J. Prasongkit, A. Grigoriev, B. Pathak, R. Ahuja, and R. H. Scheicher, J. Phys. Chem. C **117**, 15421 (2013).
[28]G. Nesher, A. Vilan, H. Cohen, D. Cahen, F. Amy, C. Chan, J. Hwang, and A. Kahn, J. Phys. Chem. B **110**, 14363 (2006).
[29]P. Ardalan, G. Dupont, and C. B. Musgrave, J. Phys. Chem. **115**, 7477 (2011).
[30]W. Wang, G. Lee, M. Huang, R. M. Wallace, and K. Cho, J. Appl. Phys. **107**, 103720 (2010).
[31]D. Murdick, X. Zhou, H. Wadley, and D. Nguyen-Manh, J. Phys. Condens. Matter **17**, 6123 (2005).
[32]X. Huang, E. Lindgren, and J. R. Chelikowsky, Phys. Rev. B Condens. Matter **71**, 165328 (2005).
[33]M. B. Javan, Phys. Lett. A **376**, 3241 (2012).
[34]Y. Zhao, *et al.*, Nat. Nanotechnol. **9**, 466 (2014).
[35]S. Inoue, R. Kuroda, X. Yin, M. Sato, and S. Kasai, Jpn. J. Appl. Phys. **54**, 04DN07 (2015).
[36]X. Zhang and S. Ptasinska, J. Phys. Chem. C **118**, 4259 (2014).
[37]M. Matmor, G. A. Lengyel, W. S. Horne, and N. Ashkenasy, Phys. Chem. Chem. Phys. **19**, 5709 (2017).